

# A Green's function approach to local rf heating in interventional MRI

Christopher J. Yeung and Ergin Atalar<sup>a)</sup>

Departments of Biomedical Engineering and Radiology, Johns Hopkins University School of Medicine, Baltimore, Maryland 21205

(Received 28 August 2000; accepted for publication 9 February 2001)

Current safety regulations for local radiofrequency (rf) heating, developed for externally positioned rf coils, may not be suitable for internal rf coils that are being increasingly used in interventional MRI. This work presents a two-step model for rf heating in an interventional MRI setting: (1) the spatial distribution of power in the sample from the rf pulse (Maxwell's equations); and (2) the transformation of that power to temperature change according to thermal conduction and tissue perfusion (tissue bioheat equation). The tissue bioheat equation is approximated as a linear, shift-invariant system in the case of local rf heating and is fully characterized by its Green's function. Expected temperature distributions are calculated by convolving (averaging) transmit coil specific absorption rate (SAR) distributions with the Green's function. When the input SAR distribution is relatively slowly varying in space, as is the case with excitation by external rf coils, the choice of averaging methods makes virtually no difference on the expected heating as measured by temperature change ( $\Delta T$ ). However, for highly localized SAR distributions, such as those encountered with internal coils in interventional MRI, the Green's function method predicts heating that is significantly different from the averaging method in current regulations. In our opinion, the Green's function method is a better predictor since it is based on a physiological model. The Green's function also elicits a time constant and scaling factor between SAR and  $\Delta T$  that are both functions of the tissue perfusion rate. This emphasizes the critical importance of perfusion in the heating model. The assumptions made in this model are only valid for local rf heating and should not be applied to whole body heating. © 2001 American Association of Physicists in Medicine. [DOI: 10.1118/1.1367860]

Key words: MRI safety, rf heating, SAR, interventional MRI

## I. INTRODUCTION

With the advent of interventional MRI, researchers and clinicians are attempting to perform procedures such as biopsies and catheterizations under MRI guidance. These procedures require the use of minimally invasive surgical devices such as catheters and guidewires for vascular applications and biopsy needles for biopsies. This presents an increased risk over a standard diagnostic MRI, primarily with respect to rf heating. Even if a device is not ferromagnetic, it has the potential to concentrate the electromagnetic (EM) field from the rf transmitter, which may substantially increase rf heating in its vicinity.<sup>1-4</sup>

Even with potentially increased rf heating, the risk of an MRI procedure may be considerably less than other imaging modalities, such as x-ray fluoroscopy. Fluoroscopic procedures have been known to last several hours and cause severe skin burns in patients, as well as expose clinicians to ionizing radiation. It would be unfortunate if a patient were prevented from having an interventional MRI procedure, with its superior soft tissue contrast, for fear of *potential* local rf heating and then sent to a conventional x-ray fluoroscopic exam where skin burning was a *certainty*. Clearly, then, it is important to thoroughly understand rf heating in an interventional MRI setting.

Current regulations for local rf heating were developed in the era of diagnostic imaging. An MR exam is considered

safe if it complies with either of these two regulations governing SAR and temperature:<sup>5,6</sup>

- (1) SAR does not exceed 8 W/kg in the head and trunk or 12 W/kg in the extremities when averaged over a gram of tissue for 15 min.
- (2) Temperature changes do not exceed 1 °C in the head, 2 °C in the trunk, or 3 °C in the extremities.

The regulations mention that local tissue damage can occur at temperatures above 43 °C and this is used as a rationale for the limits on the temperature changes by assuming a baseline temperature of 37 °C and applying factors of safety.<sup>7,8</sup> However, a rationale is not provided for the relationship between the SAR and temperature limits, nor are reasons provided for the seemingly arbitrary choice of averaging size and duration.<sup>5,6</sup>

The goal of this work is to present a model that will allow a meaningful correlation between the SAR and temperature guidelines for local rf heating, with particular respect to the highly localized EM fields associated with interventional devices. This work will show that current guidelines may be suitable for dealing with the relatively slowly varying EM fields produced by rf transmit coils situated outside the body. However, these guidelines are unsuitable for the highly concentrated rf heating that is possible with transmitting coils

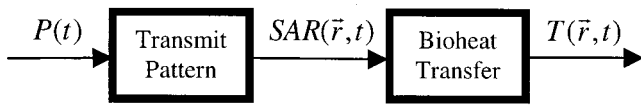


FIG. 1. Flow chart model of rf heating in MRI.

positioned inside the body or when an internal metallic device electrically couples to an external transmitter.

## II. THEORY

### A. The problem of rf heating

The determination of rf heating can be described as a two-step process as depicted in Fig. 1. The input,  $P$ , is the rf pulse of the imaging sequence and is a function of time,  $t$ . This is converted into a spatial distribution of deposited power, or specific absorption rate (SAR), depending on the coil geometry and the electromagnetic properties of the tissue including the electrical conductivity,  $\sigma$ , and permittivity,  $\epsilon$ . SAR is a function of space,  $\mathbf{r}$ , and time. This deposited power is transformed into temperature,  $T$ , distributions depending on the thermal properties of the tissue, including thermal conductivity and perfusion rates.

### B. Modeling

The first system is accurately modeled with Maxwell's equations to find the electric field in the sample. Conductive losses in the sample give rise to power deposition in the sample. This power deposition is often given in units of W/kg and called the specific absorption rate (SAR). It can be calculated from the electric field according to the following equation:

$$\text{SAR} = \frac{\sigma E^2}{\rho_t}, \quad (1)$$

where  $E$  is the rms amplitude of the electric field,  $\sigma$  is the electrical conductivity, and  $\rho_t$  is the mass density of the tissue. This is a linear, shift-invariant system with respect to the time variable, but the spatial distribution can be quite complex because of coil and patient geometry.

The second system can be modeled with the tissue bioheat equation first proposed by Pennes:<sup>9</sup>

$$\frac{1}{\alpha} \frac{dT(\mathbf{r}, t)}{dt} = \nabla^2 T(\mathbf{r}, t) - \frac{\rho_t \rho_b c_b m}{k} (T(\mathbf{r}, t) - T_b) + \frac{\rho_t}{k} \text{SAR}(\mathbf{r}, t) + Q, \quad (2)$$

where  $\alpha$  is the thermal diffusivity,  $\nabla$  is the Laplacian operator,  $\rho_t$  is the mass density of the tissue,  $\rho_b$  is the mass density of the perfusing blood,  $c_b$  is the heat capacity of the blood,  $m$  is the volumetric flow rate of blood per unit mass of tissue,  $k$  is the thermal conductivity,  $T_b$  is the temperature of the perfusing blood, and  $Q$  is the heat generated by normal chemical processes in the body. If it is assumed that metabolic heat generation maintains the core temperature at a steady level

equal to the temperature of the perfusing blood, this equation can be rewritten in terms of a temperature change  $\Delta T = T - T_b$  as follows:

$$\frac{1}{\alpha} \frac{d\Delta T(\mathbf{r}, t)}{dt} = \nabla^2 \Delta T(\mathbf{r}, t) - v^2 (\Delta T(\mathbf{r}, t)) + \frac{\rho_t}{k} \text{SAR}(\mathbf{r}, t), \quad (3)$$

where  $v^2 = \rho_t \rho_b c_b m / k$ . This is also a linear system with SAR as the input and temperature,  $T$ , as the output.

These two basic models have been widely used in the field of cancer hyperthermia.<sup>10</sup>

## III. METHODS

As an example of how to apply this model, we examined the rf heating produced when transmitting with a catheter antenna inserted into a patient. This device<sup>11</sup> has been shown to be useful for catheter tracking, and signal localization.<sup>12-16</sup> We have previously examined the transmit power distribution of the catheter antenna and have shown that the induced heating is highly localized near the device.<sup>17</sup>

First, the SAR distribution of the transmitting rf coil was determined. For simple geometries, Maxwell's equations can be solved analytically. Otherwise, numerical solutions must be used. The simple geometry of the antenna allows its electric field distribution to be computed analytically for a perfect half-wave antenna as shown by King and Harrison.<sup>18</sup> The antenna was approximated as a perfect dipole in an infinite homogeneous conductive medium. The constitutive parameters used were  $\epsilon_r = 80$  and  $\sigma = 0.8$  S/m. These values are representative of human tissue at 64 MHz. For these tissue parameters, each pole's length was set to 9.2 cm to make it a perfect half-wave.<sup>18</sup> It is important to note that wavelength in a lossy medium depends on both the permittivity and conductivity of the medium. The antenna radius was set to 0.2 mm, also a representative value.

For comparison, we also examined a model for an externally applied excitation. A uniform magnetic field excitation was applied to an infinitely long cylinder of homogeneous lossy medium. The SAR distributions in this case were previously described by Bottomley and Andrew.<sup>19</sup> Again, the constitutive parameters used were  $\epsilon_r = 80$  and  $\sigma = 0.8$  S/m.

Next, these two SAR distributions were converted to temperature distributions according to the bioheat equation. In general, analytical solutions to this partial differential equation are not possible. However, when considering only *local* heating, it is possible to achieve approximate analytical solutions under certain simplifying assumptions:

- (1) Constitutive thermal parameters ( $\alpha$ ,  $k$ ,  $v$ ) are constant in the local region of interest and over the small temperature range.
- (2) The region of interest is small compared to the whole body and is not near the surface so the infinite boundary condition can be used.

Under these assumptions, the bioheat equation can be treated as a linear shift-invariant system and is therefore fully characterized by its impulse response function or Green's

TABLE I. Green's functions,  $G$ , of the tissue bioheat equation in cylindrical (line source) and spherical (point source) polar coordinates.  $R$  is distance from point source;  $r$  is distance from line source;  $t$  is time;  $\alpha$  is thermal diffusivity;  $\rho_t$  is the mass density of the tissue;  $v$  is a lumped perfusion parameter,  $k$  is the thermal conductivity;  $K_0$  is the modified Bessel function of the second kind and order zero (Ref. 31).

Steady-state cylindrical	$G(r) = \frac{\rho_t}{2\pi k} K_0(vr)$
Steady-state spherical	$G(R) = \frac{\rho_t}{4\pi k R} e^{-vR}$
Time-dependent cylindrical	$G(r,t) = \frac{\rho_t}{4\pi k t} e^{-(r^2/4\alpha t)} e^{-av^2 t}$
Time-dependent spherical	$G(R,t) = \frac{\alpha \rho_t}{k(4\pi \alpha t)^{3/2}} e^{-(R^2/4\alpha t)} e^{-av^2 t}$

function. Green's functions are a convenient way to describe thermal problems<sup>20,21</sup> and have been applied to the bioheat equation.<sup>22,23</sup>

The Green's function was found using transform methods<sup>24,25</sup> by solving the tissue bioheat equation with an impulsive power input. Green's functions,  $G$ , are listed in Table I for cylindrical (line source) and spherical (point source) coordinates in both time-dependent and steady-state cases. Gao, Langer, and Corry showed the time-dependent and steady-state solutions for a point source in an infinite homogeneous medium.<sup>23</sup> The cylindrical (line source) solutions can be derived with the same method. Additionally, the consistency of the solutions can be verified since the steady-state solutions are equal to the definite integral of the time-dependent solutions with respect to time from zero to infinity.

To find the temperature distribution resulting from a given power source, the characteristic SAR distribution for the transmitting coil is convolved with the Green's function of the bioheat equation. Some functions can be convolved with analytical transform methods but most functions must be convolved numerically.

For the example, we used a MATLAB (The MathWorks, Inc., Natick, MA) implementation to perform the convolution in Cartesian coordinates,  $x$  and  $y$ , but with the output in cylindrical coordinate,  $r$ :

$$\Delta T(r) = \sum_i \sum_j G(i\Delta x, j\Delta y) \text{SAR}(r - i\Delta x, j\Delta y) \Delta x \Delta y. \quad (4)$$

The sampled power function, SAR, and Green's function,  $G$ , were appropriately shifted, multiplied, and summed over indices  $i$  and  $j$ , to perform the convolution. The functions were sampled at increasing resolutions,  $\Delta x$  and  $\Delta y$ , and extents (both functions are analytically infinite in extent) until doubling the resolution or extent of the functions had less than a 1% effect on the final result.

The physiological parameters used for the calculation were values for normal skeletal muscle ( $k = 0.4 \text{ W/m}^\circ\text{C}$ ) at rest ( $m = 2.7 \text{ ml}/100 \text{ g}/\text{min}$ ), and vasodilated, such as would

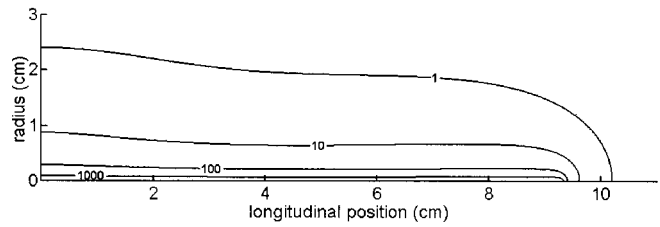


FIG. 2. Theoretical SAR distribution (W/kg) surrounding an ideal dipole antenna in lossy medium ( $\sigma = 0.8 \text{ S/m}$ ,  $\epsilon = 80$ ), normalized to 1 W input power. One quadrant is shown. Antenna is situated on longitudinal axis from  $-9.2 \text{ cm}$  to  $9.2 \text{ cm}$ .

occur in exercise or as a normal thermoregulatory response ( $m = 27 \text{ ml}/100 \text{ g}/\text{min}$ ).<sup>26</sup>

## IV. RESULTS

The complete electric field was calculated according to analytical expressions given by King and Harrison.<sup>18</sup> The SAR was then calculated according to Eq. (1) and is shown graphically in Fig. 2. It is essentially an  $e^{-2r/r^2}$  distribution (in the radial direction,  $r$ ) truncated at the origin by the spatial extent of the antenna. We have previously verified that this SAR prediction is sufficiently accurate for the evaluation of rf heating.<sup>17</sup> Since it varies so little in the longitudinal direction,  $z$ , we assume that the SAR distribution  $\text{SAR}(r,z) = \text{SAR}(r,0)$ . This simplifies the numerical calculation by reducing the dimensionality of the problem from 3D to 1.5D. Radially symmetric convolution requires a two-dimensional calculation but the output is one-dimensional. The result should accurately approximate the heating at the center of the antenna.

The 2D cylindrical steady-state Green's function was used to convert the SAR distribution to temperature. The temperature distributions shown in Fig. 3 were computed

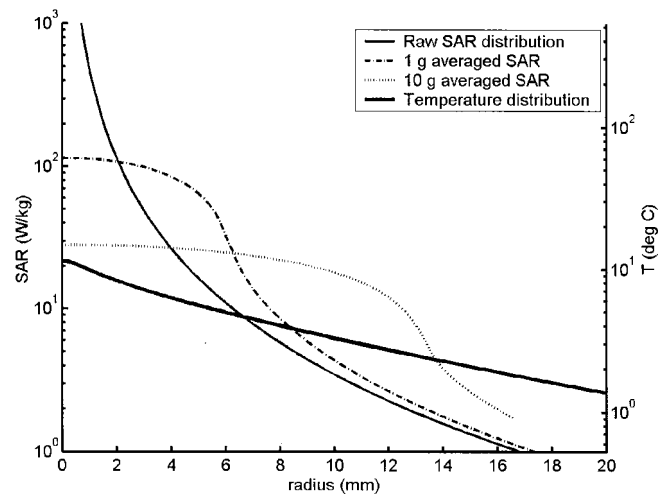


FIG. 3. Predicted SAR and steady-state temperature distributions when transmitting with a catheter antenna (radius=0.2 mm), normalized to 1 W input power. Temperature and SAR scales are aligned based on the scaling factor of the Green's function. Green's function parameters: resting muscle perfusion  $2.7 \text{ ml}/100 \text{ g}/\text{min}$ ; thermal conductivity  $0.4 \text{ W/m}^\circ\text{C}$ . The time constant for this perfusion level is 37 min.

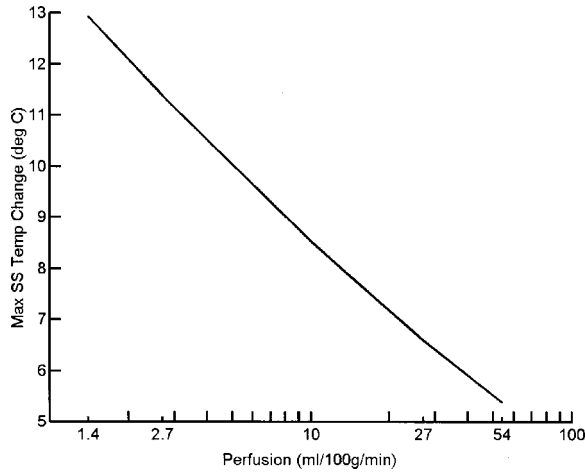


FIG. 4. Prediction of maximum steady-state temperature change when transmitting with a catheter antenna as a function of perfusion (normalized for 1 W input power). Perfusion values range from 1.4 ml/100 g/min for bone to 54 ml/100 g/min for brain. Thermal conductivity is 0.4 W/m °C. Maximum temperature rise occurs at surface of antenna.

with a spatial resolution of 0.1 mm and a Green's function spatial extent of 5 cm. To avoid convolution artifacts, power function spatial extent was twice the Green's function extent. Figure 3 compares the input SAR function to the output temperature function. It also compares the Green's function "averaging" with the arithmetic averaging approach prescribed by current regulations. For illustration, 1 g and 10 g spheres were used.

The theoretical peak temperature depends on the tissue parameters used for the Green's function. Figures 4 and 5 plot peak temperature as a function of the perfusion and thermal conductivity parameters, respectively. These figures show that the expected peak steady-state temperature decreases nonlinearly with both increasing perfusion and thermal conductivity. The absolute values on the temperature scale of these figures should not be alarming since the input

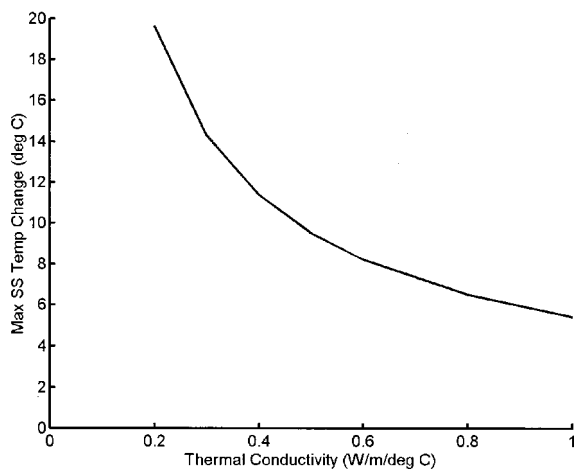


FIG. 5. Prediction of maximum steady-state temperature change when transmitting with a catheter antenna as a function of thermal conductivity (normalized for 1 W input power). Perfusion is 2.7 ml/100 g/min.

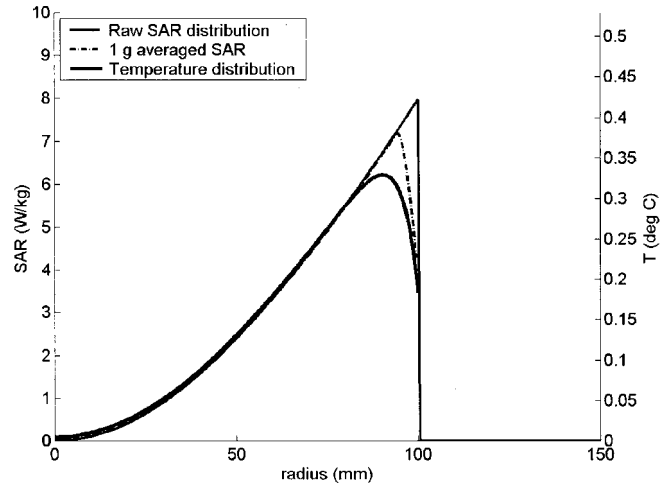


FIG. 6. SAR and steady-state temperature distributions for external field excitation of an infinitely long cylinder of homogeneous lossy medium. SAR distribution is normalized to 8 W/kg peak. Temperature scale aligned to SAR scale based on appropriate gain of Green's function. Green's function parameters: exercising muscle perfusion 27 ml/100 g/min; thermal conductivity 0.4 W/m °C.

power has been normalized to 1 W. A typical scan will use much less input power and the steady-state temperatures will therefore be scaled down appropriately.

Figure 6 shows an averaging comparison for the externally applied field. As Bottomley and Andrew have shown, the electric field has a modified Bessel function distribution which is very close to linear over the domain of the problem.<sup>19</sup> Thus, the SAR distribution is essentially quadratic. The raw SAR distribution has been normalized in Fig. 6 so that the peak SAR is 8 W/kg at the surface of the 10 cm radius medium. Averaging methods and parameters were the same as those used for Fig. 3.

## V. DISCUSSION

### A. SAR averaging

The results of Figs. 3 and 6 clearly demonstrate the effect that the choice of averaging methods has on the expected resultant distribution. When the input SAR distribution is relatively slowly varying, as is the case with external excitation of a homogeneous phantom, the choice of averaging methods has little effect on the outcome (Fig. 6). The outcome is very different, however, for highly localized SAR distributions, such as those encountered in interventional situations. Figure 3 shows that simple arithmetic averaging over an arbitrarily sized sphere of tissue can produce estimates of rf heating that are significantly different than those predicted by the more realistic tissue bioheat equation when the input SAR function is highly localized.

Let us emphasize that Green's function averaging should not normally occur at the boundary of the sample as demonstrated in Fig. 6, since the assumptions are not valid in this case. This figure is simply used to illustrate that, away from the boundary, the choice of averaging functions makes little difference, even for quadratic functions. As such, current

TABLE II. Perfusion rates and implied scaling factors (A) and implied time constants (B) for selected physiological situations.

Tissue type	Perfusion (ml/100 g/min)	A. Scaling factor (W/kg/°C)	B. Time constant (min)
	$m$	$\rho_b c_b m$	$c_t / \rho_b c_b m$
Bone (27)	1.4	1.0	71
Resting skeletal muscle (Refs. 26, 27)	2.7	1.9	37
Fat (Ref. 27)	3.7	2.6	27
Skeletal muscle (Ref. 28)	3.9–39	2.7–27	26–2.6
Skin (Ref. 27)	9.8	6.9	10.2
Skin (Ref. 28)	11–780	7.7–550	9.1–0.13
Exercising skeletal muscle (Ref. 26)	27	19	3.7
Brain (Refs. 26, 28)	54	38	1.8
Liver (Ref. 28)	58	41	1.7
Cardiac muscle (Ref. 28)	83–600	58–420	1.2–0.17
Kidney (Ref. 28)	420	300	0.24

guidelines may be suitable for external coils. However, the result of Fig. 3 clearly shows that they may not be suitable in an interventional MRI situation.

### B. Temperature to SAR scaling factor

It is possible to show temperature and SAR distributions on the same axes in Figs. 3 and 6 because the Green's function provides an inherent temperature to SAR scaling factor. If the Green's function were to be applied to a constant unit SAR distribution, the temperature distribution would also be constant, but scaled by the total integral under the function. This integral is equal to  $\rho_t/kv^2$  or  $1/\rho_b c_b m$ . This is a function of perfusion and not of thermal conductivity. Therefore, perfusion rates imply a scaling factor and vice versa. Table II shows the equivalent perfusion rates and scaling factors for a variety of physiological situations, assuming the perfusing blood has a density of  $1000 \text{ kg/m}^3$  and a heat capacity of  $4200 \text{ J/kg } ^\circ\text{C}$ , similar to water.<sup>27,28</sup>

Current regulatory guidelines use a ratio of  $4 \text{ W/kg}$  to  $1 \text{ }^\circ\text{C}$  in the trunk and limbs, which implies a perfusion rate of  $5.4 \text{ ml/100 g/min}$ , a rate twice that of resting muscle.<sup>26</sup> In the head, the guidelines use a ratio of  $8 \text{ W/kg}$  to  $1 \text{ }^\circ\text{C}$ , which implies a perfusion rate of  $10.8 \text{ ml/100 g/min}$ , a value five times less than normal brain perfusion of  $54 \text{ ml/100 g/min}$ .

### C. Time constants

We have presented only steady-state solutions to the tissue bioheat equation since we have, to date, been unable to reliably perform the necessary 3D convolution due to computational constraints. However, examination of the time-dependent Green's functions can provide an insight into the general transient behavior of the bioheat transfer system. Both the spherical and cylindrical functions have complex dependencies on the time variable. One of these dependencies is a simple decaying exponential ( $e^{-av^2t}$ ). As such,  $1/av^2$  or  $c_t/\rho_b c_b m$  is a time constant of the system. Again, this is a function only of perfusion, not of conductivity. This time constant is tabulated for different values of perfusion, again assuming blood density of  $1000 \text{ kg/m}^3$  and blood and

tissue heat capacity of  $4200 \text{ J/kg } ^\circ\text{C}$ , similar to water. Athey described the same thermal time constant arising from the bioheat equation, using a similar approach.<sup>29</sup>

As described earlier, the perfusion rate implied by the SAR to temperature conversion factor in current regulatory guidelines is  $5.4 \text{ ml/100 g/min}$ . Incidentally, this corresponds to a time constant of  $15 \text{ min}$ , the same as the currently prescribed averaging duration.

### D. Perfusion and thermal conductivity

Figures 4 and 5 show the sensitivity of the steady-state peak temperature to the thermal parameters used in the system. Both exhibit nonlinear relationships. Perfusion can be considered more important, though, since its dynamic range is much larger.

### E. SAR versus temperature

By examining the two-step rf heating model, it is clear that both SAR and temperature are important measures when reporting results to the scientific community, but they must be reported appropriately. The transmit power system depends on the electrical characteristics of the sample and the geometry of the coil. These factors can be adequately simulated in a phantom experiment. The bioheat transfer system depends on the thermal characteristics of the tissue, especially perfusion, which are not easily simulated in a phantom. Therefore, reporting temperature changes in phantom experiments, in which no perfusion exists, and concluding that the same temperature rises should be expected for *in vivo* experiments makes little sense. Rather, SAR should be reported, ideally normalized to the transmit power amplitude for easy comparison to other studies, for phantom experiments. Temperature should only be reported for *in vivo* experiments in which all the proper conditions exist.

### F. The ultimate measure of safety: Temperature or tissue damage?

This work has focused on the conversion of SAR into temperature through the tissue bioheat equation. It does not

address the fundamental issue of thermal safety: avoiding tissue damage. In whole body rf heating, the primary issue is the increase of core temperature and its potential systemic adverse effects. As such, a limit on core temperature rise is suitable. In local rf heating, the primary issue is the potential for acute thermal injury or burns. In this case, arbitrary limits on temperature are less meaningful since relatively large temperature changes may not cause burns, provided they are of short duration, and smaller temperature changes may cause burns, provided they persist long enough. Thus, for local rf safety, a measure of tissue damage that combines the effects of elevated temperature and duration should be used. Moritz and Henriques developed such a measure when studying the time/temperature relationship to the onset of skin burns.<sup>30</sup> A similar approach can be used for rf thermal safety in an MRI environment. In this case, the time-dependent Green's functions would be used to generate temperature distributions as a function of space and time. Knowing the time course of the temperature distributions will allow an estimate of tissue damage during an MR exam.

### G. Experimental verification

We have thus far presented only a theoretical model for rf heating. Experimental verification of the model is necessary to ensure that the assumptions made in simplifying the bio-heat equation are acceptable. We expect that the largest divergence of experimental data from the theoretical prediction will be due to tissue heterogeneity. Nonetheless, this theoretical analysis has clearly elucidated several important thermal parameters, namely the scaling and time constants, that should be useful for developing rational guidelines for local rf heating in MRI.

### H. Whole body heating

As a final note, it should be emphasized that the rules of thumb developed here should not be applied when evaluating whole body heating since they were developed using assumptions that apply only to local rf heating.

## VI. CONCLUSIONS

When the input SAR distribution is relatively slowly varying in space, as is the case with excitation by external rf coils, the choice of averaging methods makes virtually no difference on the expected heating as measured by temperature change. However, for highly localized SAR distributions, such as those encountered with internal coils in interventional MRI, the Green's function method predicts heating that is significantly different from the averaging method in current regulations.

We have presented a detailed, two-step method for evaluating local rf heating in an MRI environment. The primary innovation of this work is the introduction of Green's function averaging for highly localized heating sources and its inherent temperature to SAR scaling factor, which is a function of tissue perfusion. This should provide a meaningful rationale for local rf heating regulatory guidelines. The aver-

aging techniques described should be particularly useful for the evaluation of interventional MRI devices. The model also indicates that for safety studies, SAR should be reported for phantom experiments and temperature reported for *in vivo* experiments. Further study is required to determine the thresholds for acute local thermal injury (burns), which may be the ultimate determinant of thermal safety, rather than a simple temperature threshold.

## ACKNOWLEDGMENTS

This work was supported by grants from Surgi-Vision Inc. and the National Institutes of Health (R01 HL61672). The authors thank Whit Athey for helpful comments and suggestions and Mary McAllister for help in manuscript preparation. C.J.Y. is supported by the Whitaker Foundation and an NIH Training Grant. E.A. is a co-founder and shareholder of Surgi-Vision Inc. and has a potential conflict of interest.

<sup>a)</sup>Corresponding author: Department of Radiology, John Hopkins University, Outpatient Center Room 4241, 601 N. Caroline St., Baltimore, MD 21287-0845, Tel.: (401) 955-9625, Fax: (410) 614-1977, Electronic mail: eataral@mri.jhu.edu

<sup>1</sup>S. E. Maier, S. Wildermuth, R. D. Darrow, R. D. Watkins, J. F. Debatin, and C. L. Dumoulin, "Safety of MR tracking catheters," in Proc. ISMRM, 3rd Scientific Meeting, Nice, p. 497 (1995).

<sup>2</sup>S. Wildermuth, C. L. Dumoulin, T. Pfammatter, S. E. Maier, E. Hofmann, and J. F. Debatin, "MR-guided percutaneous angioplasty: Assessment of tracking safety, catheter handling and functionality," Cardiovasc. Intervent. Radiol. **21**, 404-10 (1998).

<sup>3</sup>M. E. Ladd, H. H. Quick, P. Boesiger, and G. C. McKinnon, "Rf heating of actively visualized catheters and guidewires," in Proc. ISMRM, 6th Scientific Meeting, Sydney, p. 473 (1998).

<sup>4</sup>M. K. Konings and C. J. G. Bakker, "Intolerable heating by resonating rf waves around guidewires," in Proc. ISMRM, 7th Scientific Meeting, Philadelphia, p. 1004 (1999).

<sup>5</sup>U.S. Department of Health and Human Services, Food and Drug Administration, Center for Devices and Radiological Health, "Guidance for the submission of premarket notifications for magnetic resonance diagnostic devices" (US DHHS FDA, Rockville, MD, 1998).

<sup>6</sup>International Electrotechnical Commission, "Medical electrical equipment—Part 2: Particular requirements for the safety of magnetic resonance equipment for medical diagnosis," International Standard 60601-2-33 (International Electrotechnical Commission, Geneva, 1995).

<sup>7</sup>P. Czernski and T. W. Athey, "Safety of magnetic resonance *in vivo* diagnostic examinations: theoretical and clinical considerations" (Center for Devices and Radiological Health, Rockville, MD, 1987).

<sup>8</sup>T. W. Athey, "Current FDA guidance for MR patient exposure and considerations for the future," Ann. N.Y. Acad. Sci. **649**, 242-257 (1992).

<sup>9</sup>H. H. Pennes, "Analysis of tissue and arterial temperatures in the resting human forearm," J. Appl. Physiol. **1**, 93-122 (1948).

<sup>10</sup>J. W. Strohbehn, B. S. Temby, and E. B. Douple, "Blood flow effects on the temperature distributions from an invasive microwave antenna array used in cancer therapy," IEEE Trans. Biomed. Eng. **29**, 649-661 (1982).

<sup>11</sup>O. Ocali and E. Atalar, "Intravascular magnetic resonance imaging using a loopless catheter antenna," Magn. Reson. Med. **37**, 112-118 (1997).

<sup>12</sup>E. Atalar, D. L. Kraitchman, B. Carkhuff, J. Lesho, O. Ocali, M. Solaiyappan, M. A. Guttman, and H. K. Charles, Jr., "Catheter-tracking FOV MR fluoroscopy," Magn. Reson. Med. **40**, 865-872 (1998).

<sup>13</sup>X. Yang and E. Atalar, "Intravascular MR-guided balloon angioplasty using an MR imaging-guidewire: A feasibility study in rabbits," Radiology **217**, 501-506 (2000).

<sup>14</sup>P. Aksit, J. A. Derbyshire, and E. Atalar, "Simultaneous acquisition of multiple FOV images for real time catheter tracking," in Proc. ISMRM, 8th Scientific Meeting, Denver, p. 158 (2000).

<sup>15</sup>J. M. Serfaty, E. Atalar, J. DeClerck P. Karmarkar, H. H. Quick, K. A. Shunk, A. W. Heldman, and X. Yang, "Real time projection MR angiog-

- raphy with intra-arterial injections of gadolinium," in Proc. ISMRM, 8th Scientific Meeting, Denver, p. 42 (2000).
- <sup>16</sup>B. D. Bolster, Jr., J. M. Serfaty, and E. Atalar, "In vivo measurement of pulsewave velocity in small vessels using intravascular MRI," *Magn. Reson. Med.* **45**, 53–60 (2001).
- <sup>17</sup>C. J. Yeung and E. Atalar, "Rf transmit power limit for the barewire loopless catheter antenna," *J. Magn. Reson. Imaging* **12**, 86–91 (2000).
- <sup>18</sup>R. W. P. King and C. W. Harrison, Jr., *Antennas and Waves: A Modern Approach* (M.I.T., Cambridge, 1969), pp. 252–258.
- <sup>19</sup>P. A. Bottomley and E. R. Andrew, "Rf magnetic field penetration, phase shift and power dissipation in biological tissue: Implications for NMR imaging," *Phys. Med. Biol.* **23**, 630–643 (1978).
- <sup>20</sup>H. S. Carslaw and J. C. Jaeger, *Conduction of Heat in Solids*, 2nd ed. (Oxford University Press, Oxford, 1959), pp. 353–386.
- <sup>21</sup>R. Haberman, *Elementary Applied Partial Differential Equations*, 3rd ed. (Prentice Hall, Upper Saddle River, NJ, 1998), pp. 370–433.
- <sup>22</sup>R. Vyas and M. L. Rustgi, "Green's function solution to the tissue bioheat equation," *Med. Phys.* **19**, 1319–1324 (1992).
- <sup>23</sup>B. Gao, S. Langer, and P. M. Corry, "Applications of the time-dependent Green's function and Fourier transforms of the solution of the bioheat equation," *Int. J. Hyperthermia* **11**, 267–285 (1995).
- <sup>24</sup>L. Debnath, *Integral Transforms and Their Applications* (CRC, Boca Raton, 1995), pp. 200–201.
- <sup>25</sup>R. N. Bracewell, *The Fourier Transform and Its Applications* (McGraw-Hill, New York, 1986), pp. 241–253.
- <sup>26</sup>A. W. Guy, J. F. Lehmann, and J. B. Stonebridge, "Therapeutic applications of electromagnetic power," *Proc. IEEE* **62**, 55–75 (1974).
- <sup>27</sup>B. I. Tropea and R. C. Lee, "Thermal injury kinetics in electrical trauma," *J. Biomech. Eng.* **114**, 241–250 (1992).
- <sup>28</sup>A. Shitzer and R. C. Eberhart, "Heat generation, storage, and transport processes," in *Heat Transfer in Medicine and Biology*, edited by A. Shitzer and R. C. Eberhart (Plenum, New York, 1985), p. 141.
- <sup>29</sup>T. W. Athey, "A model of the temperature rise in the head due to magnetic resonance imaging procedures," *Magn. Reson. Med.* **9**, 177–184 (1989).
- <sup>30</sup>A. R. Moritz and F. C. Henriques, Jr., "Studies of thermal injury II: The relative importance of time and surface temperature in the causation of cutaneous burns," *Am. J. Pathol.* **23**, 695–720 (1947).
- <sup>31</sup>M. Abramowitz and I. A. Stegun, *Handbook of Mathematical Functions, with Formulas, Graphs, and Mathematical Tables* (Dover, Mineola, 1977), p. 374.